

Article

Polyoxometalates Encapsulated into Hollow Periodic Mesoporous Organosilica as Nanoreactors for Extraction Oxidation Desulfurization

Yan Gao ^{1,*} , Yu Chen ¹, Cuiying Wang ¹, Aiping Yin ¹, Hailong Li ¹ and Jianshe Zhao ²¹ Department of Chemistry, Xinzhou Normal University, Xinzhou 034000, China² College of Chemistry & Materials Science, Northwest University, Xi'an 710069, China

* Correspondence: gaoyan202109@126.com; Tel.: +86-0350-3339205

Abstract: In this work, the highly active polyoxometalate (PW₂Mo₂) with Venturrello structure and its corresponding catalyst were applied in catalytic desulfurization for the first time. PW₂Mo₂ as an active component was effectively encapsulated in hollow periodic mesoporous organosilica (HPMOS) to form the nanoreactor PW₂Mo₂@HPMOS, where the central cavity and mesoporous shell facilitate mass transfer and both provide a stable place to react with organic sulfides. Desulfurization test results show that the hollow nanoreactor PW₂Mo₂@HPMOS can almost remove four sulfides simultaneously from diesel in 2 h under mild conditions. Besides, the nanocatalyst PW₂Mo₂@HPMOS can be reused and recycled for at least seven consecutive tests without any noticeable loss in performance. With the rapid development of the economy, the massive use of sulfur-containing fuel has a huge impact on the global climate. After combustion of sulfur-containing fuel, the realized SO_x is an important inducement of the formation of acid rain, and the realized sulfur particle is also a major source of haze. Therefore, removing sulfur compounds from fuel is an important issue that needs to be solved immediately.

Keywords: polyoxometalates; hollow periodic mesoporous organosilica; nanoreactor; desulfurization; chemical process



Citation: Gao, Y.; Chen, Y.; Wang, C.; Yin, A.; Li, H.; Zhao, J.

Polyoxometalates Encapsulated into Hollow Periodic Mesoporous Organosilica as Nanoreactors for Extraction Oxidation Desulfurization. *Catalysts* **2023**, *13*, 747. <https://doi.org/10.3390/catal13040747>

Academic Editors: Mufisir Kuniyil, Mohammed Rafi Shaik and Syed Farooq Adil

Received: 22 February 2023

Revised: 7 April 2023

Accepted: 10 April 2023

Published: 14 April 2023



Copyright: © 2023 by the authors. Licensee MDPI, Basel, Switzerland. This article is an open access article distributed under the terms and conditions of the Creative Commons Attribution (CC BY) license (<https://creativecommons.org/licenses/by/4.0/>).

1. Introduction

With the development of the economy and the improvement of people's living standards, the demand for fuel oil has increased rapidly [1,2]. From 2010 to 2020, China's apparent total consumption of refined oil products (gasoline, diesel, and kerosene) increased from 246 million tons to 289 million tons. Global fuel oil demand will continue to grow strongly over the next few years. However, the large amount of sulfur oxides emitted by fuel combustion causes a series of environmental problems, such as acid rain and haze [3,4]. Therefore, in order to improve the environment and reduce pollution, it is urgent to desulfurize fuel and use low sulfur or even sulfur-free fuel. At present, most countries in the world have adopted increasingly strict sulfur emission policies to eliminate the harm caused by sulfur oxides [5–8]. Even so, it is still necessary to develop efficient and convenient desulfurization technology to produce ultra-low sulfur or even sulfur-free fuel.

The most common industrial technology for desulfurization of crude oil is hydrodesulfurization [9,10]. However, this method needs to operate under extreme conditions (high temperature and high pressure), which requires sufficient energy and high production costs, as well as potentially unsafe hydrogen. In this respect, alternative non-hydrodesulfurization technologies, such as the oxidative method, extraction method, adsorption method, and so on, have become urgent research topics. Extraction oxidation desulfurization (EODS) technology is a new efficient method that combines extraction desulfurization and oxidation desulfurization [11,12]. In the extraction oxidative desulfurization process, the sulfides in the diesel are transferred to the extraction layer, where they are oxidized to sulfones until

the diesel is sulfide-free. The extraction oxidation desulfurization technology overcomes the complex two-step operation of the traditional oxidation separation technology, which requires oxidation first and then removal, and the defects of the low efficiency of pure extraction desulfurization. One of the key points of EODS is the selection and preparation of a high activity catalyst.

Some metal-containing materials, such as polyoxometalates composed of Venturello anions and organic cations, have attracted extensive interest from researchers due to their excellent catalytic activity and have been widely used in various catalytic oxidation reactions [13–17]. At the same time, polyoxometalate, with its simple preparation, stable structure, and lack of pollution, is considered an economic and environmental desulfurization catalyst. It was shown by Wenshuai Zhu and co-workers that the dibenzothiophene (DBT) can be completely oxidized to the corresponding sulfone within 2 h under the catalyze of polyoxometalate catalyst $[(n-C_8H_{17})_3NCH_3]_3[PO_4\{WO(O_2)_2\}_4]$ [18]. Salet S. Balula's research group prepared the supported catalyst by embedding the active ingredient $(nBu_4N)_3\{PO_4[WO(O_2)_2]_4\}$ in the SBA-15 channel through a simple impregnation method. The catalyst could achieve a desulfurization efficiency of 100%, but its reusability remains to be improved [19]. A large number of studies have shown that polyoxometalate has high desulfurization activity but is difficult to recycle due to its solubility in organic solvents. Loading or encapsulating the active component onto carrier material can improve its reusability while ensuring its high activity.

The good support material can not only improve the reusability of the catalyst but also disperse the active components well and prevent them from agglomerating. Suitable pore size, a large specific surface area, and a stable structure are the factors to be considered in the selection of support materials. In recent years, metal-organic frame materials, carbon materials, mesoporous silicon materials, and so on have aroused people's interest. Among them, the hollow periodic mesoporous organosilica (HPMOS) is a new kind of organic-inorganic hybrid material with a central cavity and an ordered mesoporous shell, which has a great potential for application in many fields, such as catalysis, drug delivery, chromatographic separation, sensing, drug release, insulation, and fuel cells [20–22]. And due to its characteristics of high specific surface area, adjustable pore size, ordered mesoporous channel, and central hole, it is a promising candidate material for nanoreactors with remarkable catalytic performance [23]. In theory, HPMOS, as a nanoreactor, can well accommodate the active component, and its cavity and mesoporous shells are conducive to mass transfer. Significantly, the nanoreactor allows the catalytic reaction to take place in a confined space where the substrate can effectively contact the active site, resulting in a significant increase in catalytic activity.

In this work, Venturello structure polyoxometalate $(TBA)_3[PO_4\{W_2Mo_2O_{20}\}] \cdot 6H_2O$, denoted PW_2Mo_2 , was encapsulated into the mesoporous of HPMOS to form a catalytic nanoreactor $PW_2Mo_2@HPMOS$, which was used for desulfurization of multicomponent model diesel. The prepared nanoreactor $PW_2Mo_2@HPMOS$ showed excellent catalytic activity for the EODS in the presence of H_2O_2 , and almost all sulfides (BT, DBT, 4-MDBT, 4,6-DMDBT) were removed simultaneously from diesel in 2 h under mild conditions. At the same time, the excellent reusability of the nanoreactor also indicates that the confined effect of the mesoporous shell contributes to solidifying the active component.

2. Experimental Section

2.1. Materials

Sodium molybdate (99%), disodium hydrogen phosphate (99%), sodium tungstate (99%), tetrabutylammonium chloride (TBAC, 97%), cetyltrimethylammonium bromide (CTAB, 98%), benzothiophene (BT, 95%), dibenzothiophene (DBT, 98%), 4-methyldibenzothiophene (4-MDBT, 96%), 4,6-dimethyldibenzothiophene (4,6-DMDBT, 97%), and tetradecane (99%), butyl-3-methylimidazolium hexafluorophosphate ($[Bmim]PF_6$, 97%), and 1,2-Bis(triethoxysilyl)ethane (BTSE, 96%) were bought from Aladdin Co., Ltd., Shanghai, China, Octane (99.9%) and

30% aqueous hydrogen peroxide (H_2O_2) were purchased from Tianjing Fuchen chemical reagent factory.

2.2. Catalyst Preparation

2.2.1. Preparation of PW_2Mo_2

Firstly, the α -Keggin-type heteropolyacid $\text{H}_3\text{PW}_6\text{Mo}_6\text{O}_{40}\cdot n\text{H}_2\text{O}$ was synthesized according to the method based on published procedures [24]. Then, the peroxoheteropoly species $[\text{PO}_4\{\text{W}_2\text{Mo}_2\text{O}_{20}\}]^{3-}$ was prepared by oxidizing $\text{H}_3\text{PMo}_6\text{W}_6\text{O}_{40}\cdot n\text{H}_2\text{O}$ with H_2O_2 . The detailed process is as follows [25–27]: 30% aq. H_2O_2 (10 mL) was poured into an aqueous solution of $\text{H}_3\text{PMo}_6\text{W}_6\text{O}_{40}\cdot n\text{H}_2\text{O}$ (0.5 mmol) under magnetic stirring at room temperature. After stirring for 60 min, 3 mL of an aqueous solution containing tetrabutylammonium chloride (1.6 mmol) was added while fiercely stirring. After reaction, the resultant precipitate $(\text{TBA})_3[\text{PO}_4\{\text{W}_2\text{Mo}_2\text{O}_{20}\}] \cdot 6\text{H}_2\text{O}$, denoted PW_2Mo_2 , was separated by vacuum filtration, washed with distilled water for three times, and dried overnight at $50\text{ }^\circ\text{C}$.

PW_2Mo_2 . Anal. Calcd. (%) for $(\text{TBA})_3[\text{PO}_4\{\text{W}_2\text{Mo}_2\text{O}_{20}\}] \cdot 6\text{H}_2\text{O}$ (1813.48): C, 30.85; H 6.56; N 2.26. ICP anal. (g/kg): W, 399.23; Mo, 210.67. Selected FT-IR (cm^{-1}): 2963 (s), 2873 (s), 1485 (s), 1387 (m), 1076 (s), 1043 (w), 971 (s), 870 (s), 795 (w), 740 (w), 661 (s), 589 (s), 543 (s), and 430 (m).

2.2.2. Preparation of Hollow Periodic Mesoporous Organosilica (HPMOS)

HPMOS was prepared using a one-step method. Firstly, CTAB (0.64 g) was poured into a mixed solution of ethanol (30 mL), ammonia (2 mL), and distilled water (150 mL) under magnetic stirring to obtain a transparent solution. Secondly, a mixture of ethanol (30 mL), BTSE (0.48 g), and octane (0.02 mL) was added to the above transparent solution. After stirring for 60 min, the white product was formed, collected by centrifugation, and washed with distilled water three times. Thirdly, the solid was transferred to a 100 mL ethanol solution containing 1 mL hydrochloric acid and heated at $80\text{ }^\circ\text{C}$ for 6 h; this step was repeated three times to fully remove CTAB. Finally, the product HPMOS was collected by centrifugation, washed with distilled water and ethanol, and then dried at $60\text{ }^\circ\text{C}$ for 6 h.

HPMOS. Selected FT-IR (cm^{-1}): 1640 (m), 1419 (w), 1274 (m), 1166 (s), 1038 (s), 913 (m), 773 (m), 701 (m), and 454 (m).

2.2.3. Preparation of Composite $\text{PW}_2\text{Mo}_2@\text{HPMOS}$

The hollow nanoreactor $\text{PW}_2\text{Mo}_2@\text{HPMOS}$ was prepared by the facile impregnation method. HPMOS (0.5 g) was poured into a 5 mL acetonitrile solution containing active component PW_2Mo_2 (0.3 g) at room temperature under magnetic stirring for 24 h. Then the product was collected by centrifugation and washed with acetonitrile three times, and dried at $60\text{ }^\circ\text{C}$ for 12 h.

$\text{PW}_2\text{Mo}_2@\text{HPMOS}$. ICP anal. (g/kg): W, 36.24; Mo, 18.74. Selected FT-IR (cm^{-1}): 1640 (m), 1462 (m), 1419 (w), 1384 (m), 1276 (s), 1166 (s), 1038 (m), 913 (m), 775 (m), 770 (m), and 454 (m).

2.3. Characterizations

Inductively coupled plasma mass spectrometry (ICP-MS) was performed on the PerkinElmer NexION 300 \times instrument to analyze the metal content of samples. Fourier transform infrared (FT-IR) spectra of different samples were carried out on an EQUINOX 55 spectrometer using the KBr pellet method with a wavenumber range of $4000\text{--}400\text{ cm}^{-1}$. X-ray diffraction (XRD) patterns of high-angle and low-angle were measured on a Bruker D8 Advance diffractometer and a Shimadzu XRD-7000S, respectively. Thermogravimetric curves were recorded on a NETZSCH STA 449A thermal analyzer from $30\text{--}1000\text{ }^\circ\text{C}$ with a heating rate of $5\text{ }^\circ\text{C}/\text{min}$. N_2 adsorption-desorption isotherms were collected on the TriStar II 3020 sorption analyzer at 77 K. Scanning electron microscopy (SEM) with electron energy dispersive spectroscopy (EDS) and transmission electron microscopy (TEM) were tested

on the SU 8010 instrument and the Talos F200X instrument to analyze the morphology of samples. A gas chromatogram was carried out on the Agilent 7890 to detect the change in sulfide concentration during the reaction.

2.4. Catalytic Testing

A certain amount of BT, DBT, 4-MDBT, and 4,6-DMDBT in n-octane simultaneously to prepare a multicomponent simulated diesel with a total sulfide concentration of 2000 ppm, in which the single component concentration was 500 ppm. A typical desulfurization test was performed in a 5 mL closed borosilicate reactor including 0.75 mL simulated diesel, 0.75 mL extractant ([Bmim]PF₆), a certain amount of catalyst, and 0.3 mmol H₂O₂, which was equipped with a magnetic stirrer and soaked in a 70 °C constant temperature oil bath. Extractive oxidation desulfurization consists of two processes: raw materials were first mixed and stirred for 10 min, then an oxidizing agent (H₂O₂) was added to activate the oxidation process. Both processes were carried out at 70 °C with stable magnetic stirring. Residual sulfide concentration in fuel oil at different times was detected by GC analysis using tetradecane as the internal standard.

During the reusability test of the catalyst, the catalyst was separated, washed, and dried after each cycle. Then, the recovered catalyst, fresh model diesel, extractant, and oxidant were added to the reactor to start the next test. The recyclability of the desulfurization system was carried out by removing the desulfurized diesel at the end of the reaction and then adding fresh model diesel and oxidant to start the next cycle.

3. Results and Discussion

3.1. Catalyst Characterization

In order to test the content of the active component in the composite, the composite was examined by ICP-MS. The result confirms that the loading amount of the active component PW₂Mo₂ was 0.12 mmol/g. The functional group of synthesized materials was monitored by FT-IR spectroscopy (Figure 1). The FT-IR spectrum of PW₂Mo₂ exhibits some characteristic peaks in the 1100–540 cm⁻¹ range assigned to the Venturello structure anion, and the stretching vibration characteristic peak attributed to the O-O bond appears at 870 cm⁻¹ [28,29]. The FT-IR spectrum of HPMOS shows several strong peaks located at 1035, 773, and 454 cm⁻¹ ascribed to antisymmetric stretching vibration and symmetric stretching vibration of Si-O-Si [30,31]. The immobilization of PW₂Mo₂ was verified by the FT-IR spectrum, which showed some peaks that belonged to the active component at 1462, 1384, and 480–580 cm⁻¹.

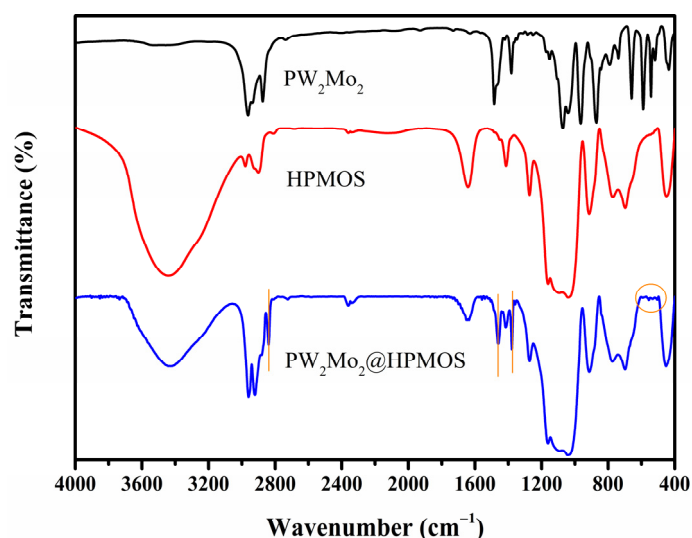


Figure 1. FT-IR spectra of PW₂Mo₂, HPMOS, and PW₂Mo₂@HPMOS.

The HPMOS before and after introducing the active component was studied by X-ray diffraction (Figure 2). The low angle XRD pattern of HPMOS shows a well-resolved peak at $2\theta = 0.89^\circ$, indicating the existence of mesoporous structures on the hollow silicon shell [32,33]. After immobilized PW_2Mo_2 , the XRD pattern of the composite is similar to that of HPMOS, which verified that the ordered structure of HPMOS was not damaged in the synthesis process. In addition, the high-angle XRD pattern of $PW_2Mo_2@HPMOS$ did not display peaks assigned to the active component, further confirming the successful introduction of the active component into the pores of the carrier material.

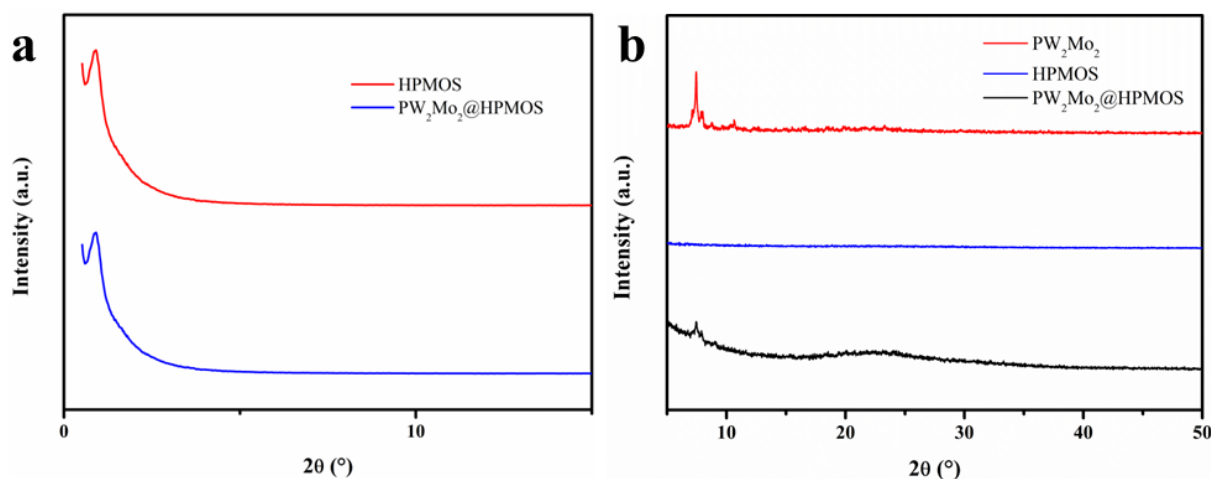


Figure 2. Low-angle (a) and high-angle (b) XRD patterns of prepared materials.

Figure 3 exhibits the thermal stability of the $PW_2Mo_2@HPMOS$ composite, pure HPMOS, and PW_2Mo_2 . The TG curve of PW_2Mo_2 shows four weight-loss processes: the first step, losing 7.0% mass from room temperature to $171^\circ C$, is due to the removal of adsorbed water and solvent; the second step, from $171^\circ C$ with 25.6% mass loss, may be attributed to the decomposition of a cation the third stage occurs at $262^\circ C$, losing 18.1% mass, which is due to the decomposition of the anion; and the last stage, from $406^\circ C$ with 17.7% mass, the dehydration-condensation reaction. The total weight loss of HPMOS is 15.6%, which is due to solvent volatilization, template decomposition, and Si-OH condensation. The TG curve of the composite $PW_2Mo_2@HPMOS$ is similar to that of PW_2Mo_2 , and the total weight loss is 22.9%, which is consistent with the result of ICP-MS.

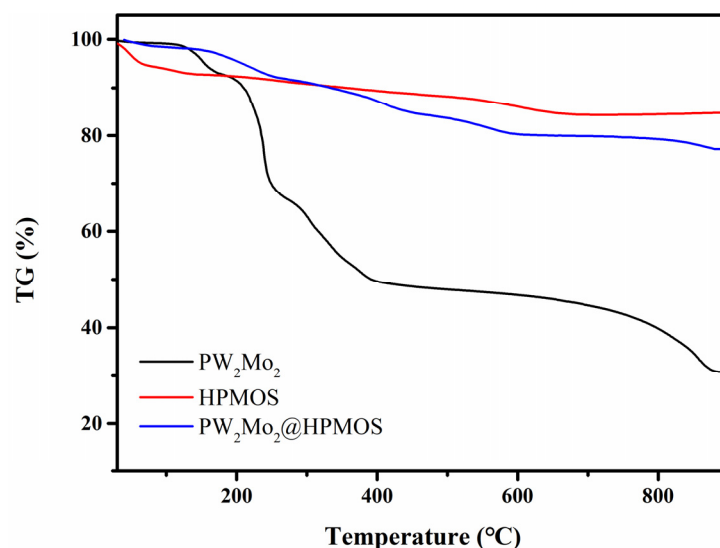


Figure 3. TG curves of PW_2Mo_2 , HPMOS, and $PW_2Mo_2@HPMOS$.

The mesoporous structure of pure HPMOS and composite $PW_2Mo_2@HPMOS$ was researched through nitrogen adsorption-desorption isotherm measurements (Figure 4, Table 1). HPMOS and $PW_2Mo_2@HPMOS$ both show type IV adsorption-desorption isotherms, indicating the presence of characteristic porous structures. Meanwhile, the H4-type hysteresis loops in the p/p_0 range of 0.45–1.0 are observed in the two isotherms, which further proves that the materials have microporous and mesoporous structure (Figure 4a). In addition, the results show that the HPMOS has a high specific surface area ($942.05\text{ m}^2/\text{g}$) and a large pore volume ($1.45\text{ cm}^3/\text{g}$), and the pore size mainly concentrates at 2.0–3.7 nm and 3.7–5.2 nm. Compared with HPMOS, the specific surface area and pore volume of the composite $PW_2Mo_2@HPMOS$ are lower, which is due to the pore space occupied by the active component PW_2Mo_2 . At the same time, the pore size distribution curve also shows that the pore size of $PW_2Mo_2@HPMOS$ becomes smaller due to the successful introduction of the active component (Figure 4b).

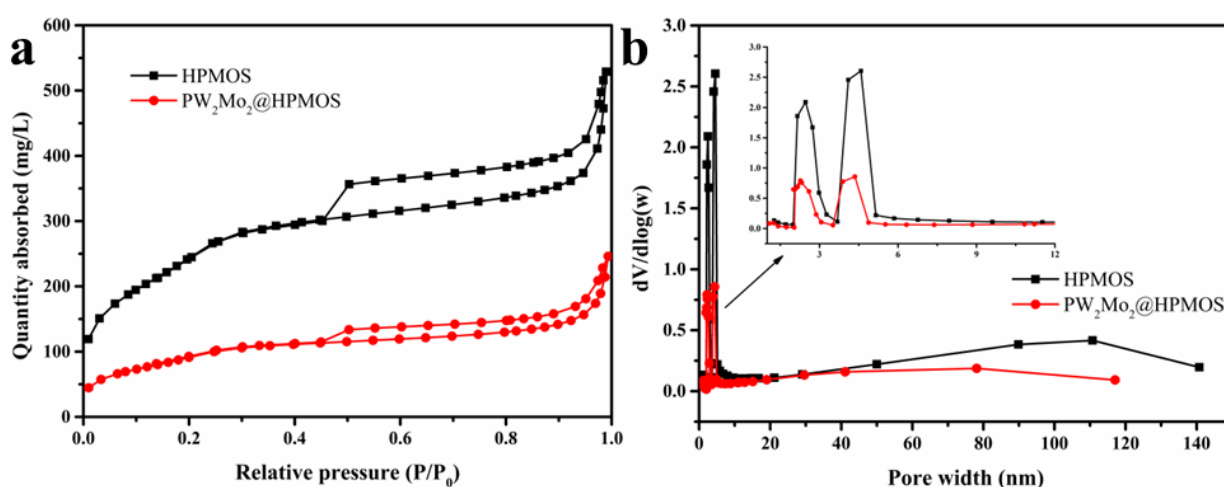


Figure 4. Nitrogen adsorption-desorption isotherms (a) and the corresponding pore size distribution curves (b) of HPMOS and $PW_2Mo_2@HPMOS$.

Table 1. The specific surface area, pore volume, and pore diameter of the samples.

Sample	S_{BET} (m^2/g)	V (cm^3/g)	D (nm)
HPMOS	942.05	1.45	5.62
$PW_2Mo_2@HPMOS$	326.46	0.48	5.88

The morphology and element distribution of the synthesized materials were analyzed by SEM, TEM, and EDX. The SEM image shows that PW_2Mo_2 is an irregularly shaped block (Figure 5a). The SEM and TEM images of HPMOS are displayed in Figure 5b,d, indicating their well-defined hollow periodic mesoporous nanosphere structure with a diameter of about 200 nm. Figure 5c,e shows that the morphology of a hollow periodic mesoporous nanosphere of composite is maintained after the immobilization of PW_2Mo_2 . As can be seen from Figure 5f–m, the mapping of the Si, O, and C elements of $PW_2Mo_2@HPMOS$ on individual nanospheres further verifies the successful formation of the internal cavity, and the mapping of the P, W, and Mo elements further confirms the successful immobilization of PW_2Mo_2 , which was distributed uniformly in the pore of the HPMOS.

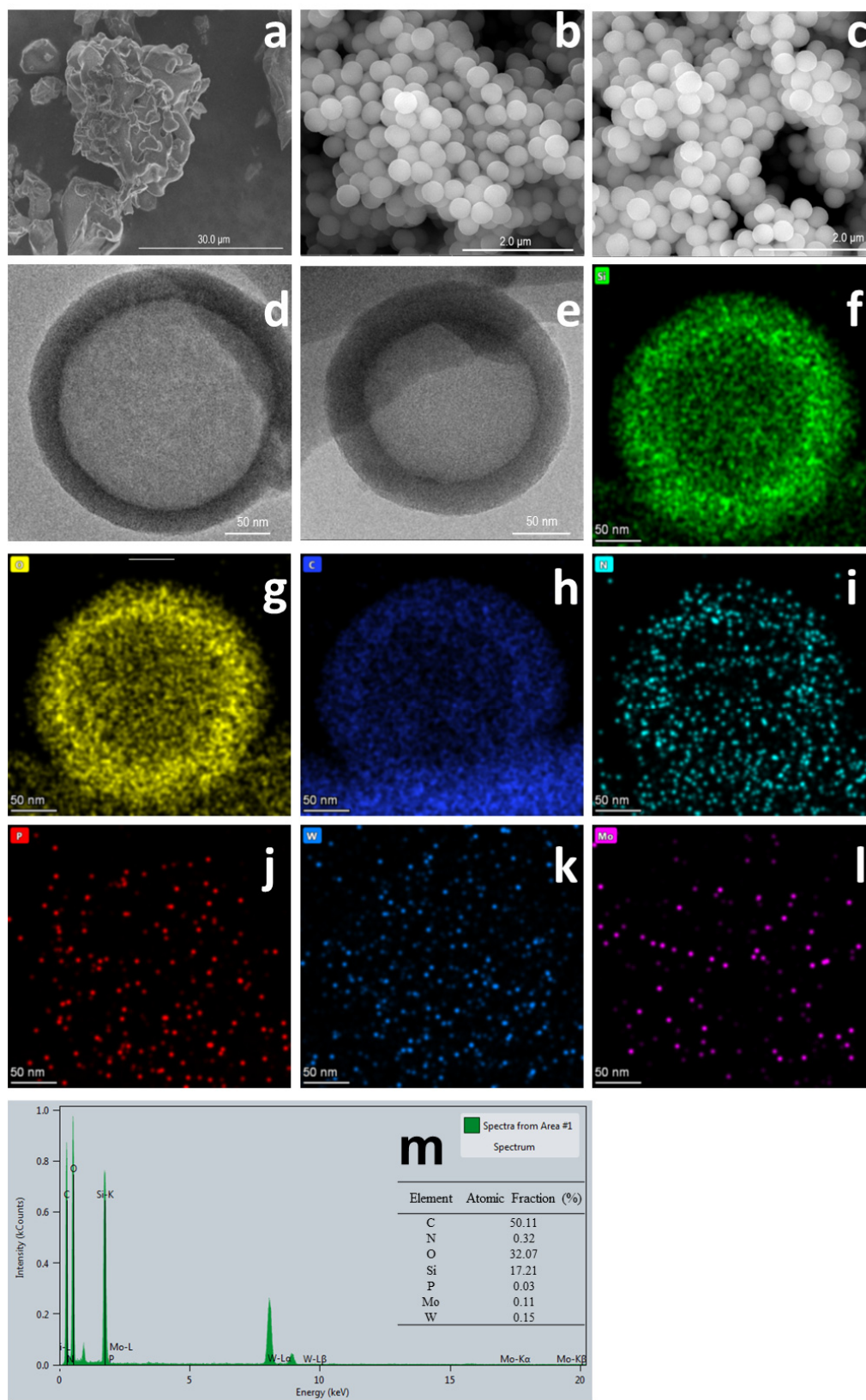


Figure 5. SEM images of PW_2Mo_2 (a), HPMOS (b), and $\text{PW}_2\text{Mo}_2@\text{HPMOS}$ (c). TEM images of HPMOS (d) and $\text{PW}_2\text{Mo}_2@\text{HPMOS}$ (e). Mapping image of $\text{PW}_2\text{Mo}_2@\text{HPMOS}$ (f–l). EDX spectrum of $\text{PW}_2\text{Mo}_2@\text{HPMOS}$ (m).

3.2. Desulfurization Efficiency Catalyzed by $PW_2Mo_2@HPMOS$ Nanoreactor

The removal of organic sulfides was carried out at 70 °C under continuous magnetic agitation in a microreactor including a certain amount of catalyst containing 5 μmol active component, 0.75 mL of multicomponent simulated diesel consisting of four refractory sulfur-containing compounds, namely BT, DBT, 4-MDBT, and 4,6-DMDBT, and an equal volume of [Bmim]PF₆ as an extractant. After stirring for ten minutes, the sulfides in the multicomponent simulated diesel were extracted into the extractant, and the extraction equilibrium was reached. Then, aqueous hydrogen peroxide (0.3 mmol) was injected as an oxidant into the reactor to activate the catalytic oxidation process.

The catalytic behavior of PW_2Mo_2 , HPMOS, and hollow $PW_2Mo_2@HPMOS$ were assessed under initial conditions, as shown in Figure 6. The result shows that HPMOS had no catalytic effect on EODS. PW_2Mo_2 and $PW_2Mo_2@HPMOS$, as homogeneous catalysts and heterogeneous hollow nanoreactors, promoted near total desulfurization of the model diesel with sulfide removal rates of 99.8% and 99.9%, respectively. In other words, the introduction of HPMOS can maintain high catalytic activity.

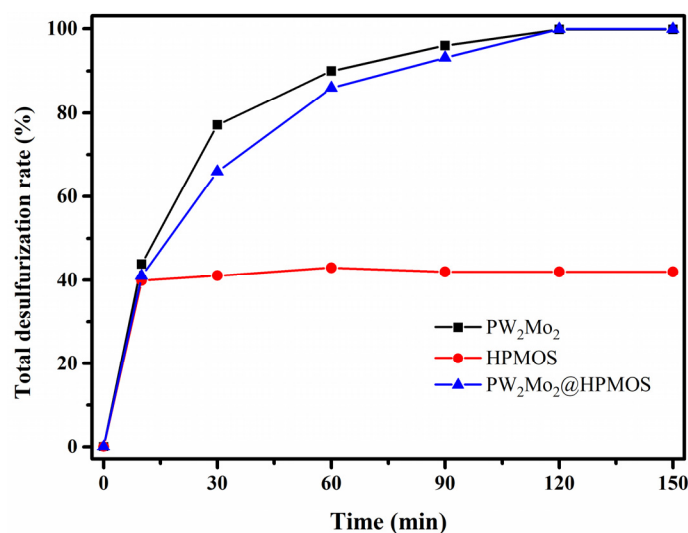


Figure 6. Desulfurization profile of a multicomponent model fuel using 5 μmol PW_2Mo_2 , 32.5 g HPMOS or $PW_2Mo_2@HPMOS$, containing 5 μmol PW_2Mo_2 , [Bmim]PF₆ extraction solvent, and H₂O₂ oxidant at 70 °C.

3.3. Condition Optimization

According to the above result, a hollow nanoreactor containing PW_2Mo_2 exhibits significant activity in the removal of four organic sulfides. Therefore, under the catalysis of $PW_2Mo_2@HPMOS$, the influence of three parameters, including catalyst dose, oxidant amount, and temperature, on the total desulfurization efficiency was carried out to achieve the best result under optimal conditions.

Using as few catalysts as possible to minimize the cost and maximize the desulfurization efficiency is the goal pursued by the industry. Therefore, the effect of catalysts containing different amounts of the active component PW_2Mo_2 was studied and shown in Figure 7a. With the amount of PW_2Mo_2 catalyst increasing from 1 μmol to 5 μmol , the total desulfurization rate improved from 67.5% to 99.9% at 120 min. Subsequently, with the PW_2Mo_2 amount increased to 7 μmol , the conversion of sulfides was almost complete. The results show that with the increase in PW_2Mo_2 amount, the content of the active molecule increases rapidly and the reaction rate increases. At the same time, when the sulfide conversion reached its peak, increasing the catalytic dose had no significant effect on the reaction. Therefore, the optimal content of the active component PW_2Mo_2 was 5 μmol .

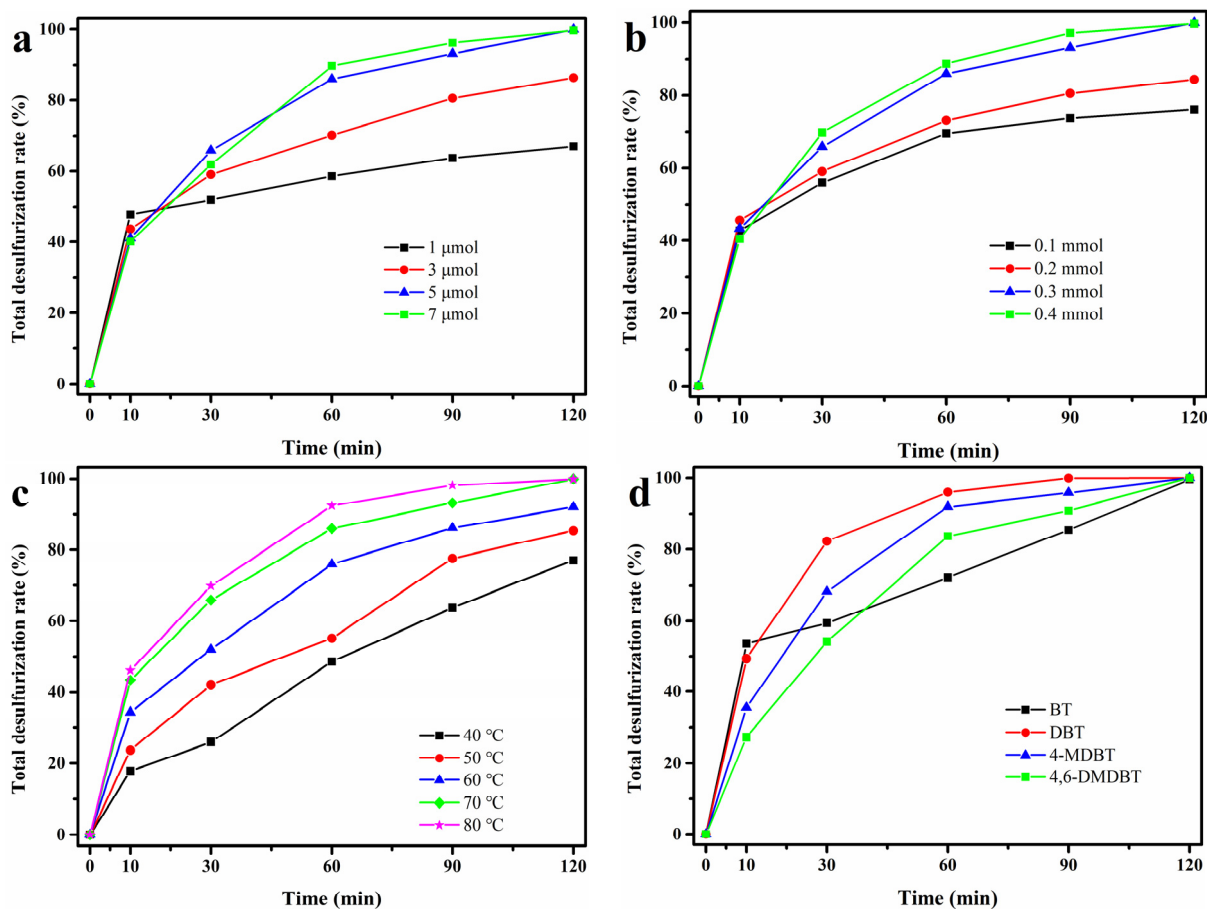


Figure 7. Desulfurization profile of a multicomponent model fuel catalyzed by $PW_2Mo_2@HPMOS$ containing different amounts of PW_2Mo_2 using 0.3 mmol H_2O_2 at 70 °C (a); the effect of H_2O_2 amount on EODS catalyzed by $PW_2Mo_2@HPMOS$ containing 5 μmol of PW_2Mo_2 at 70 °C (b); the effect of temperature on EODS catalyzed by $PW_2Mo_2@HPMOS$ containing 5 μmol of PW_2Mo_2 using 0.3 mmol H_2O_2 at 70 °C (c); desulfurization profile of four sulfides catalyzed by $PW_2Mo_2@HPMOS$ containing 5 μmol of PW_2Mo_2 using 0.3 mmol H_2O_2 at 70 °C (d).

H_2O_2 , as an oxidant, plays an important role in the catalytic oxidation of sulfides (Figure 7b). An increase in the H_2O_2 dose from 0.1 mmol to 0.4 mmol leads to an improvement in the total desulfurization rate. When the dosage of H_2O_2 reaches 0.3 mmol, the total desulfurization rate reaches the maximum value of 99.6%. The total desulfurization efficiency did not increase significantly when the amount of oxidant was increased. So, 0.3 mmol was determined to be the optimal value of the H_2O_2 dose.

Appropriately high temperatures can effectively accelerate the catalytic reaction rate, which is once again verified in this experiment (Figure 7c). When the EODS test was carried out at 40 °C, 50 °C, 60 °C, and 70 °C, the corresponding maximum desulfurization efficiency was 77.1%, 85.3%, 91.9%, and 99.9%, respectively. When the temperature continues to rise to 80 °C, the desulfurization rate is accelerated. However, considering that increasing the temperature will increase the production cost, the optimal temperature is finally determined to be 70 °C.

Under the optimum reaction conditions: a certain amount of catalyst containing 5 μmol PW_2Mo_2 , 0.3 mmol H_2O_2 , and 70 °C, the concentration of four sulfides over time was detected (Figure 7d). During the catalytic oxidation process, the order of activity in sulfur oxidation was $DBT > 4-MDBT > 4,6-DMDBT > BT$, which is affected by the electron density and steric hindrance of the sulfur atom.

3.4. Reusability of Catalyst and Recyclability of the EODS System

The reusability of the nanoreactor $PW_2Mo_2@HPMOS$ was studied for several cycles under optimal conditions. After each test, the material was separated, washed, and dried, and then added to the next test. The recyclability of the EODS system was tested by removing the desulfurized diesel after each test and then adding fresh diesel and H_2O_2 to initiate the next EODS cycle. As can be seen in Figure 8, the reusability test showed that the efficiency of the catalytic hollow nanoreactor decreased slightly to 90.6% after the seventh cycle, which may be caused by the loss of active components during the cycle. In order to detect the loss of active components in the recovered materials, ICP-MS analysis was performed. The results of ICP-MS showed that the loading amounts of active components in reused catalyst and recycled catalyst are 0.101 and 0.114 mmol/g, respectively. In comparison, the desulfurization performance of the EODS system only decreased to 95.2% after the seventh cycle due to the little or no loss of the active components. However, the increased introduction of aqueous oxidizer may hinder the transfer of sulfides from diesel to the extraction phase, resulting in a slight decrease in desulfurization efficiency. To maximize desulfurization rate under the premise of lowest cost, the pursuit of industrial applications is necessary. For industrial production, the costs can be reduced by reducing material consumption and simplifying procedures, which are characteristics of the recycling system of EODS. Therefore, the catalyst prepared in this work, possessing good recyclability and excellent activity, is expected to be applied to industrial production.

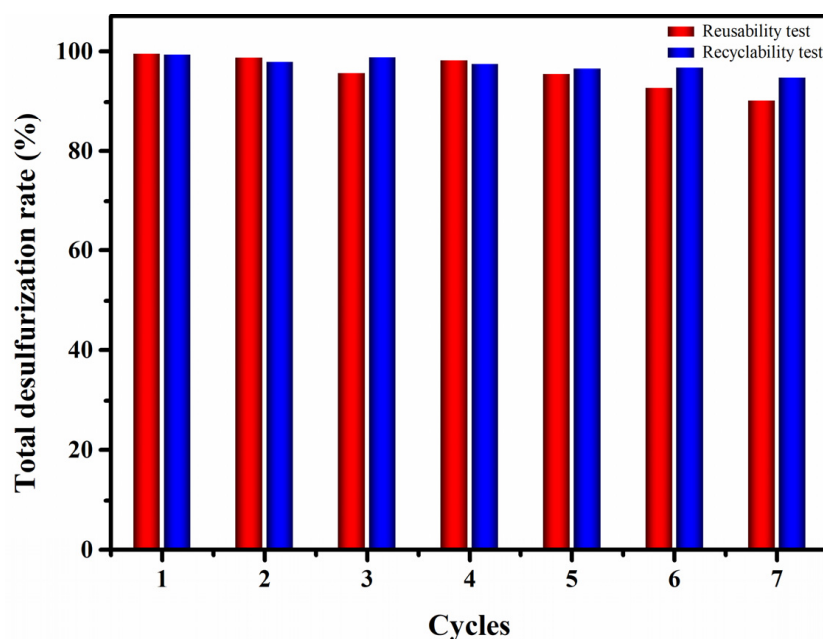


Figure 8. Reusability of catalyst $PW_2Mo_2@HPMOS$ and recyclability of the EODS system.

3.5. Stability of $PW_2Mo_2@HPMOS$ Catalyst

After seven consecutive recyclability and reusability tests, the catalytic hollow nanoreactors were separated, washed, dried, and characterized. The FT-IR spectra and SEM images of treated $PW_2Mo_2@HPMOS$ after recyclability and reusability tests maintain similar profiles to those of the fresh catalyst $PW_2Mo_2@HPMOS$ (Figure 9). The FT-IR spectrum of $PW_2Mo_2@HPMOS$ after the first cycle is similar to that of a fresh catalyst. However, some additional peaks can be observed at around 1600 cm^{-1} in the FT-IR spectra of recycled and reused samples, which may be related to sulfur compounds adsorbed on the catalyst surface [34,35]. The results show that the catalyst has excellent stability and a good industrial application prospect.

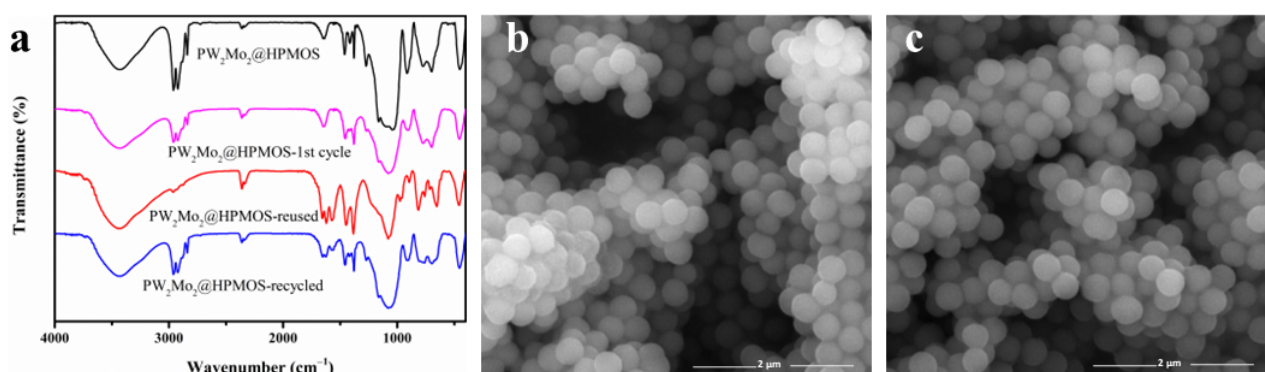


Figure 9. FT-IR spectra of reused and recycled samples (a), SEM images of a reused sample (b), and a recycled sample (c).

3.6. Comparison of Desulfurization of Fuel in a Nanoreactor

A comparison of the desulfurization results of model fuel catalyzed by different nanoreactors reported in the literature is displayed in Table 2. The data show that DBT can be almost completely removed from the fuel when it is catalyzed by different catalysts under certain conditions. It is noteworthy that catalysts $PW_2Mo_2@HPMOS$ prepared in this study can simultaneously remove multiple sulfides from fuel oil, indicating that the catalyst has a certain potential in practical application.

Table 2. Comparison of the desulfurization of fuel in the nanoreactor.

Catalyst	Substrate		Test Conditions				Desulfurization Rate, %	Reference
	Species	Concentration, ppm	Oxidant	[O]/S	T, °C	Reaction Time, min		
MoO_x/HS	DBT	200	O_2	3	50	60	99.7	[36]
	4-MDBT	200				60	99.6	
	4,6-DMDBT	200				90	39.3	
$PMo_{12}/AmHMSiO_2@C$	DBT	800	H_2O_2	6	40	180	>99	[37]
$MoO_2@GNF$	BT	125	TBHP *	20	60	120	95.3	[38]
	DBT	500					98.8	
	4,6-DMDBT	125					94.8	
MoO_3/SiO_2-1HN	DBT	500	H_2O_2	6	60	30	99.9	[39]
$PW_2Mo_2@HPMOS$	BT	500	H_2O_2	10	70	90	100.0	This work
	DBT	500				120	99.5	
	4-MDBT	500				120	100.0	
	4,6-DMDBT	500				120	99.9	

* tert-butyl hydroperoxide.

4. Conclusions

In summary, Venturello-based complexes with the unique peroxide bond PW_2Mo_2 were successfully encapsulated in hollow periodic mesoporous organosilica (HPMOS) to obtain a catalytic nanoreactor ($PW_2Mo_2@HPMOS$), which was applied to the extraction, oxidation, and desulfurization of synthetic diesel. The result shows that the $PW_2Mo_2@HPMOS$ nanoreactor displayed high activity for four refractory organic sulfides in a dual liquid phase desulfurization system using H_2O_2 as an oxidant. Under the optimized conditions, the four sulfides can be almost completely removed after 120 min of reaction, and the order of activity in sulfur oxidation during the reaction was $DBT > 4-MDBT > 4,6-DMDBT > BT$. The excellent performance is mainly attributed to the high efficiency of mass transfer in the cavity and mesoporous channel, where the sulfide can enter and exit freely, providing a place for the collision and reaction between the sulfide and the active component. In addition, the catalyst reusability test and EODS system recyclability test show that the catalyst has excellent reusability and a good industrial application prospect.

Author Contributions: Conceptualization, Y.G. and J.Z., Methodology, Y.G., Software, Y.C., C.W. and A.Y., Formal analysis, H.L. and J.Z., Data curation, Y.G., Investigation, Y.G., writing—original draft, Y.G., funding acquisition, Y.G. All authors have read and agreed to the published version of the manuscript.

Funding: This research was funded by Fundamental Research Program of Shanxi Province, grant 202103021223359; Scientific and Technological Innovation Programs (STIP) of Higher Education Institutions in Shanxi, grant 2021L453; Xinzhou Normal University Fund, grant 2021KY06; Xinzhou Normal University PhD startup fund, grant 00001045.

Data Availability Statement: Data will be made available on request.

Conflicts of Interest: The authors declare no conflict of interest.

References

1. Haruna, A.; Merican, Z.M.A.; Musa, S.G. Abubakar, Sulfur removal technologies from fuel oil for safe and sustainable environment. *Fuel* **2022**, *329*, 125370. [[CrossRef](#)]
2. Mishra, H.; Siddiqi, U.; Kumari, I.D.; Behera, S.; Mukherjee, B.C. Meikap, Pyrolysis of waste lubricating oil/waste motor oil to generate high-grade fuel oil: A comprehensive review. *Renew. Sustain. Energy Rev.* **2021**, *150*, 111446. [[CrossRef](#)]
3. Nikokavoura, A.; Trapalis, C. Graphene and g-C₃N₄ based photocatalysts for NO_x removal: A review. *Appl. Surf. Sci.* **2018**, *430*, 18–52. [[CrossRef](#)]
4. Chatrattanawet, N.; Saebea, D.; Authayanun, S.; Arpornwichanop, A.; Patcharavorachot, Y. Performance and environmental study of a biogas-fuelled solid oxide fuel cell with different reforming approaches. *Energy* **2018**, *146*, 131–140. [[CrossRef](#)]
5. Zhang, L.; Wang, J.; Sun, Y.; Jiang, B.; Yang, H. Deep oxidative desulfurization of fuels by superbase-derived Lewis acidic ionic liquids. *Chem. Eng. J.* **2017**, *328*, 445–453. [[CrossRef](#)]
6. Wu, J.; Li, Y.; Jiang, M.; Huo, Y.; Wang, X.; Wang, X. Achieving deep desulfurization with inverse-micellar polyoxometalates and oxygen. *RSC Adv.* **2021**, *11*, 9043–9047. [[CrossRef](#)]
7. Lü, J.; Fu, Y.; Wang, J.; Chen, H. Study on the desulfurization performance of calcium-based desulfurizer and NaHCO₃ desulfurizer. *Environ. Sci. Pollut. Res.* **2023**, *30*, 20357–20368. [[CrossRef](#)]
8. Ghahremani, H.; Nasri, Z.; Eikani, M.H. Ultrasound-assisted oxidative desulfurization (UAOD) of Iranian heavy crude oil: Investigation of process variables. *J. Pet. Sci. Eng.* **2021**, *204*, 108709. [[CrossRef](#)]
9. Petrova, D.; Lyubimenko, V.; Ivanov, E.; Gushchin, P.; Kolesnikov, I. Energy basics of catalytic hydrodesulfurization of diesel fuels. *Catalysts* **2022**, *12*, 1301. [[CrossRef](#)]
10. Fedushchak, T.A.; Uimin, M.A.; Maikov, V.V.; Akimov, A.S.; Zhuravkov, S.P.; Vosmerikov, A.V.; Prosvirin, I.P.; Velichkina, L.M.; Stepanov, A.A.; Kogan, V.M. Novel molybdenite-based nanopowder catalysts for hydrodesulfurization. *Pet. Chem.* **2021**, *61*, 794–805. [[CrossRef](#)]
11. Huo, Q.; Liu, G.; Sun, H.; Fu, Y.; Ning, Y.; Zhang, B.; Zhang, X.; Gao, J.; Miao, J.; Zhang, X.; et al. CeO₂-modified MIL-101(Fe) for photocatalysis extraction oxidation desulfurization of model oil under visible light irradiation. *Chem. Eng. J.* **2021**, *422*, 130036. [[CrossRef](#)]
12. Harandi, M.S.; Shams, E.; Sharifi, E.; Momenbeik, F. A new approach in deep desulfurization of model fuel through integration of electrochemical oxidation and liquid-liquid extraction in a biphasic system. *Sep. Purif. Technol.* **2021**, *275*, 119087. [[CrossRef](#)]
13. Nojima, S.; Kamata, K.; Suzuki, K.; Yamaguchi, K.; Mizuno, N. Selective oxidation with aqueous hydrogen peroxide by [PO₄{WO(O₂)₂]₄]³⁻ supported on zinc-modified tin dioxide. *ChemCatChem* **2015**, *7*, 1097–1104. [[CrossRef](#)]
14. Kamata, K.; Sugahara, K.; Ishimoto, R.; Nojima, S.; Mizuno, N. Highly selective epoxidation of cycloaliphatic alkenes with aqueous hydrogen peroxide catalyzed by [PO₄{WO(O₂)₂]₄]³⁻/imidazole. *Chemcatchem* **2014**, *6*, 2327–2332. [[CrossRef](#)]
15. Han, W.; Yang, Y.; Fang, D.; Zang, S. Application of 12-heteropolyacids of molybdenum and tungsten ([Smim]₃[PMoW₃O₂₄]) in epoxidation of olefins. *Oxid. Commun.* **2014**, *37*, 112–120.
16. Zhang, L.; Ji, X.; Ren, X.; Ma, Y.; Shi, X.; Tian, Z.; Asiri, A.M.; Chen, L.; Tang, B.; Sun, X. Electrochemical Ammonia Synthesis via Nitrogen Reduction Reaction on a MoS(2) Catalyst: Theoretical and Experimental Studies. *Adv. Mater.* **2018**, *30*, e1800191. [[CrossRef](#)]
17. Zhang, L.; Liang, J.; Wang, Y.; Mou, T.; Lin, Y.; Yue, L.; Li, T.; Liu, Q.; Luo, Y.; Li, N.; et al. High-Performance Electrochemical NO Reduction into NH(3) by MoS(2) Nanosheet. *Angew. Chem. Int. Ed. Engl.* **2021**, *60*, 25263–25268. [[CrossRef](#)] [[PubMed](#)]
18. Rafiee, E.; Eavani, S. Organic-inorganic polyoxometalate based salts as thermoregulated phase-separable catalysts for selective oxidation of thioethers and thiophenes and deep desulfurization of model fuels. *J. Mol. Catal. A Chem.* **2013**, *380*, 18–27. [[CrossRef](#)]
19. Julião, D.; Mirante, F.; Ribeiro, S.O.; Gomes, A.C.; Valença, R.; Ribeiro, J.C.; Pillinger, M.; De Castro, B.; Gonçalves, I.S.; Balula, S.S. Deep oxidative desulfurization of diesel fuels using homogeneous and SBA-15-supported peroxophosphotungstate catalysts. *Fuel* **2019**, *241*, 616–624. [[CrossRef](#)]
20. Lin, C.X.; Li, Z.; Brumbley, S.; Petrasovits, L.; Mcqualter, R.; Yu, C.; Lu, G.Q. Synthesis of magnetic hollow periodic mesoporous organosilica with enhanced cellulose tissue penetration behaviour. *J. Mater. Chem.* **2011**, *21*, 7565–7571. [[CrossRef](#)]

21. Yang, L.; Guo, H.; Wang, L.; Zhang, J. A facile “polystyrene-dissolving” strategy to hollow periodic mesoporous organosilica with flexible structure-tailorability. *Microporous Mesoporous Mater.* **2017**, *239*, 173–179. [[CrossRef](#)]
22. Qian, C.; Al-Hamyari, B.; Tang, X.; Hou, B.; Yang, S.; Zhang, G.; Lv, H.; Yang, Z.; Wang, Z.; Shi, Y. Interface-engineered paclitaxel-based hollow mesoporous organosilica nanoplatforams for photothermal-enhanced chemotherapy of tumor. *Mol. Pharm.* **2021**, *18*, 4531–4542. [[CrossRef](#)]
23. Ying, Y.A.; Feng, Y.A.; Hai, W.B.; Bz, A.; Sh, A. Amine-promoted Ru1/Fe₃O₄ encapsulated in hollow periodic mesoporous organosilica sphere as a highly selective and stable catalyst for aqueous levulinic acid hydrogenation. *J. Colloid Interface Sci.* **2021**, *581*, 167–176. [[CrossRef](#)]
24. Li, S.W.; Gao, R.M.; Zhang, R.L.; Zhao, J.S. Template method for a hybrid catalyst material POM@MOF-199 anchored on MCM-41: Highly oxidative desulfurization of DBT under molecular oxygen. *Fuel* **2016**, *184*, 18–27. [[CrossRef](#)]
25. Furukawa, H.; Nakamura, T.; Inagaki, H.; Nishikawa, E.; Imai, C.; Misono, M. Oxidation of cyclopentene with hydrogen peroxide catalyzed by 12-heteropoly acids. *Chem. Lett.* **1988**, *24*, 877–880. [[CrossRef](#)]
26. Yan, G.; Dj, A.; Dfs, A.; Bdc, A.; Jz, B.; Ssb, A. A simple desulfurization process to achieve high efficiency, sustainability and cost-effectivity via peroxotungstate catalyst. *Mol. Catal.* **2021**, *505*, 1–7. [[CrossRef](#)]
27. Salles, L.; Thouvenot, R.; Brégeault, J. Redistribution and fluxionality in heteropolyoxoperoxo complexes: [PO₄{M₂O₂(-O₂)₂(O₂)₂}]³⁻ with M = Mo and/or W. *Dalton Trans.* **2004**, *6*, 904. [[CrossRef](#)]
28. Zhu, W.; Zhu, G.; Li, H.; Chao, Y.; Zhang, M.; Du, D.; Wang, Q.; Zhao, Z. Catalytic kinetics of oxidative desulfurization with surfactant-type polyoxometalate-based ionic liquids. *Fuel Process. Technol.* **2013**, *106*, 70–76. [[CrossRef](#)]
29. Zhu, W.; Zhu, G.; Li, H.; Chao, Y.; Chang, Y.; Chen, G.; Han, C. Oxidative desulfurization of fuel catalyzed by metal-based surfactant-type ionic liquids. *J. Mol. Catal. A Chem.* **2011**, *347*, 8–14. [[CrossRef](#)]
30. Zhou, W.; Ma, H.; Dai, Y.; Du, Y.; Guo, C.; Wang, J. Architecture of nanoantioxidant based on mesoporous organosilica trp-met-PMO with dipeptide skeleton. *Materials* **2023**, *16*, 638. [[CrossRef](#)]
31. Teng, S.; Han, Y.; Hu, Y.; Li, J.; Wang, M.; Guo, Z.; Yang, W. Swellable hollow periodic mesoporous organosilica capsules with ultrahigh loading capacity for hydrophobic drugs. *J. Colloid Interface Sci.* **2023**, *630*, 266–273. [[CrossRef](#)]
32. Huo, H.; Jiang, Y.; Zhao, T.; Wang, J.; Li, D.; Xu, X.; Lin, K. Periodic Mesoporous Organosilicas as Efficient Nanoreactors in Cascade Reactions Preparing Cyclopropanic Derivatives. *Chem. Asian J.* **2019**, *14*, 1496–1505. [[CrossRef](#)] [[PubMed](#)]
33. Haghghat, M.; Shirini, F.; Golshekan, M. Efficiency of NaHSO₄ modified periodic mesoporous organosilica magnetic nanoparticles as a new magnetically separable nanocatalyst in the synthesis of [1,2,4]triazolo quinazolinone/pyrimidine derivatives. *J. Mol. Struct.* **2018**, *1171*, 168–178. [[CrossRef](#)]
34. Ribeiro, S.O.; Nogueira, L.S.; Gago, S.; Almeida, P.L.; Corvo, M.C.; Castro, B.d.; Granadeiro, C.M.; Balula, S.S. Desulfurization process conciliating heterogeneous oxidation and liquid extraction: Organic solvent or centrifugation/water? *Appl. Catal. A Gen.* **2017**, *542*, 359–367. [[CrossRef](#)]
35. Mirante, F.; Dias, L.; Silva, M.; Ribeiro, S.O.; Corvo, M.C.; de Castro, B.; Granadeiro, C.M.; Balula, S.S. Efficient heterogeneous polyoxometalate-hybrid catalysts for the oxidative desulfurization of fuels. *Catal. Commun.* **2018**, *104*, 1–8. [[CrossRef](#)]
36. Jiang, W.; Xiao, J.; Gao, X.; An, X.; Li, H. In situ fabrication of hollow silica confined defective molybdenum oxide for enhanced catalytic oxidative desulfurization of diesel fuels. *Fuel* **2021**, *305*, 121470. [[CrossRef](#)]
37. Liu, H.; Li, Z.; Dong, J.; Liu, D.; Liu, C.; Chi, Y.; Hu, C. Polyoxometalates encapsulated into hollow double-shelled nanospheres as amphiphilic nanoreactors for an effective oxidative desulfurization. *Nanoscale* **2020**, *12*, 16586–16595. [[CrossRef](#)] [[PubMed](#)]
38. Astle, M.A.; Rance, G.A.; Loughlin, H.; Peters, T.D.; Khlobystov, A.N. Molybdenum dioxide in carbon nanoreactors as a catalytic nanosponge for the efficient desulfurization of liquid fuels. *Adv. Funct. Mater.* **2019**, *29*, 1808092. [[CrossRef](#)]
39. Yang, G.; Feng, F.; Luo, Y.; Qin, J.; Yuan, F.; Wang, S.; Luo, S.; Ma, J. Facile synthesis of MoO₃ nanodots self-assembled into hollow mesoporous silica: Enhancing efficient oxidative desulfurization and investigating reaction mechanism. *J. Environ. Chem. Eng.* **2021**, *9*, 106309. [[CrossRef](#)]

Disclaimer/Publisher’s Note: The statements, opinions and data contained in all publications are solely those of the individual author(s) and contributor(s) and not of MDPI and/or the editor(s). MDPI and/or the editor(s) disclaim responsibility for any injury to people or property resulting from any ideas, methods, instructions or products referred to in the content.